Pattern Analysis and Applications (2024) 27:54
https://doi.org/10.1007/s10044-024-01280-1

THEORETICAL ADVANCES

Early detection of Alzheimer's disease using squeeze and excitation network with local binary pattern descriptor

Ambily Francis[1,2] · S. Immanuel Alex Pandian[1] · K. Martin Sagayam[1] · Lam Dang[3] · J. Anitha[4] · Linh Dinh[5] · Marc Pomplun[6] · Hien Dang[7,8]

Received: 27 August 2023 / Accepted: 15 April 2024

Abstract
Alzheimer's disease is a degenerative brain disease that impairs memory, thinking skills, and the ability to perform even the most basic tasks. The primary challenge in this domain is accurate early stage disease detection. When the disease is detected at an early stage, medical professionals can prescribe medications to reduce brain shrinkage. Although the disease may not be curable, these interventions can extend the patient's life by slowing down the rate of shrinkage. The four cognitive states of the human brain are cognitive normal (CN), mild cognitive impairment convertible (MCIc), mild cognitive impairment non-convertible (MCInc), and Alzheimer's disease (AD). Mild cognitive impairment convertible (MCIc) is the early stage of Alzheimer's disease. Individuals with MCIc will develop Alzheimer's disease for a few years. However, it is difficult to detect this state through medical investigations. The mild cognitive impairment non-convertible state (MCInc) is the state immediately before MCIc. MCInc is a common condition in people of all ages, where minor memory issues arise as a result of normal aging. Early detection of AD can be claimed if and only if the transition from MCInc to MCIc is complete. Deep learning algorithms can be promising techniques for identifying the progression stage of a disease using magnetic resonance imaging. In this study, a novel deep learning algorithm was proposed to improve the classification accuracy of MCIc vs. MCInc. This study utilized the advantages of local binary patterns along with squeeze and excitation networks (SENet). Without the squeeze and excitation network, the classification accuracy of MCIc versus MCInc was 82%. The classification accuracy improved by 86% with the use of SENet. The experimental results show that the proposed model achieves better performance for MCInc vs. MCIc classification in terms of accuracy, precision, recall, F1 score, and ROC.

Keywords Alzheimer's disease · Mild cognitive impairment convertible · Mild cognitive impairment non-convertible · Local binary pattern · Squeeze and excitation networks · Convolutional neural network

✉ Hien Dang
hiendt@tlu.edu.vn

[1] Department of Electronics and Communication, Karunya Institute of Technology and Sciences, Coimbatore, Tamil Nadu, India

[2] Department of Electronics and Communication, Sahrdaya College of Engineering and Technology, Kerala, India

[3] Department of Computer Science, INSA Lyon, Villeurbanne, France

[4] Department of Computer Science and Engineering, Karunya Institute of Technology and Sciences, Coimbatore, Tamil Nadu, India

[5] Department of Information Systems, Suffolk University, Boston, USA

[6] Department of Computer Science, University of Massachusetts, Boston, MA, USA

[7] Department of Mathematics and Computer Science, Molloy University, Rockville Centre, NY, USA

[8] Faculty of Computer Science and Engineering, Thuyloi University, Hanoi, Vietnam

Published online: 09 May 2024

1 Introduction

Alzheimer's disease (AD) is a brain syndrome that gradually abolishes memory and intellectual abilities, and the ability to perform the simplest tasks. Alzheimer's disease affects nearly 50 million individuals worldwide, as of 2020 [1]. It mostly affects people over the age of 65, although up to 10% of instances impact people in their 30s to mid-60s [2]. It affects approximately 6% of adults aged 65 years and older, with women being affected more frequently than males [3]. Accurate early diagnosis and curing methods are required to control the disease and its associated societal issues.

If early disease signs are identified before some patient experiences symptoms, there is a good chance that the patient will receive timely treatment without worsening the condition. It is extremely difficult for doctors to determine the difference between the early and late stages of the disease by using magnetic resonance imaging (MRI) and clinical testing. Many studies have applied machine learning techniques and artificial neural networks to solve problems in medical and disease diagnosis [4–6]. Recently, deep-learning algorithms have been successfully used to diagnose various diseases [7–22]. In this study, MRI scans were analyzed to determine the signs of Alzheimer's disease in its early stages. Doctors may use the successfully built system as a precisely articulated form of communication to identify AD in its early phases.

Doctors are conducting clinical tests to better understand the aberrant status of the human brain. Patients were asked to complete a questionnaire that reflected their brain abnormalities, such as Alzheimer's disease, during a mini-mental state test. The correct detection of illness necessitates frequent discussions with clinicians. Early detection of Alzheimer's disease can only be achieved by analyzing scores across multiple discourses. Subjective judgments were used to make clinical diagnoses.

Hippocampal shrinkage is a common phenomenon in aging, and an accelerated rate of hippocampal shrinkage is a reliable indicator of Alzheimer's disease. The progression of Alzheimer's disease involves various stages of cognition, which can be identified by analyzing the shrinkage of the hippocampus, the growth of ventricles in the brain, and the transition from gray matter to CSF. These factors are crucial in differentiating between mild cognitive impairment convertible (MCIc) and mild cognitive impairment non-convertible (MCInc). The rate of hippocampal shrinkage is higher in MCIc compared to MCInc. However, it may not be easy to differentiate between these two conditions using traditional MRI analysis. Deep learning algorithms can extract features from MRI images and identify patterns that may be overlooked by human analysis. Therefore, using deep learning algorithms can be a powerful tool in accurately distinguishing MCIc and MCInc, and in predicting the conversion of MCI to Alzheimer's disease.

Medical specialists are already using computer-aided methods for the diagnosis of Alzheimer's in addition to traditional clinical diagnosis. Supervised and unsupervised machine learning approaches were used to analyze the digital pathology images. Expert domain knowledge and relevant feature data are used to classify labeled data using supervised learning algorithms [23, 24]. Deep learning models can extract and understand discriminative features from available training data and can design feature extractors on their own. Transfer learning was used to increase the accuracy and computational time of the image categorization using a neural network model. Pre-trained neural networks are employed as feature extractors in transfer learning models, and the output of the pre-trained network is provided to a new classification layer trained on problem-specific data. Ensemble transfer learning models are used to improve the performance by combining multiple pre-trained models with new classification layers [25, 26]. This improves the image classification performance of the assembled models at the expense of the model complexity. The squeeze and excitation networks act on the channel attention mechanism by strengthening and weakening each feature channel without significant computational complexity. The focus of this study was on the MCIc vs. MCInc classification. The paper is structured as follows: Sect. 2 provides an exploration of related work, Sect. 3 explains the proposed methods, the model with local binary pattern, and the model with local binary pattern and SENet for early AD detection. These models are taking the advantage of stengths of local binary pattern and squeeze and excitation network. These models provide a commendable classification accuracy for MCIc vs. MCInc. Section 4 highlights the obtained results, and Sect. 5 engages in a thorough discussion of these findings. The paper concludes in Sect. 6, and Sect. 7 directs attention to potential future scope of research.

2 Related works

Deep learning algorithms have been used by researchers to develop advanced techniques for early identification of Alzheimer's disease. A stacked encoder for representing latent features was proposed in [27]. Low-level variables, such as gray matter tissue volumes, are considered by the algorithm, which improves the diagnostic accuracy for early diagnosis of Alzheimer's disease. An algorithm based on a 3D convolutional neural network and sparse autoencoder was proposed in [28]. The algorithm enhances the accuracy of three-class categorization (AD, CN, and MCI). To categorize AD, CN, and MCI [29], 2D convolutional neural

networks and a sparse autoencoder were used. Compared to the algorithm in [28], the [29] algorithm is easier because it employs 2D convolution. In contrast [29], does not take advantage of the 3D spatial information of MRI images, whereas [28] does. According to the approach in [30], non-biomedical pre-trained models, such as ResNet [31], learn cross-domain features that allow the model to extract important low-level features from MRI images to increase the classification accuracy. The proposed approach ensures that the data augmentation is efficient before learning.

For the classification of AD and CN, the method in [32] generates 3D multichannel feature maps based on voxception-Resnet. Data augmentation was performed before creating the feature maps. The algorithm was applied to diffusion MRI images. In [33], a non-biomedical pre-trained model called VGG-16 was used to learn the cross-domain features and improve accuracy. This approach provides a mathematical model based on VGG-16 transfer learning and achieves an outstanding three-class classification accuracy. The features from the sagittal, coronal, and transverse slices of MRI images were combined using the ensemble-based technique introduced in [34]. Data augmentation is performed to avoid overfitting. This algorithm uses a two-stage ensemble-learning method. In the first step, three base classifiers were used to ensemble sagittal, coronal, and transverse slices. Another base classifier ensembles three-axis slices in the second step. Each basic classifier consisted of six convolutional layers. To improve the classification accuracy, the outputs from numerous base classifiers were combined.

In [35], the algorithm was composed of three deep convolutional neural networks that were slightly distinct. The four basic operational layers of the individual model are as follows:1) convolution, 2) batch normalization, 3) rectified linear unit, and 4) pooling. The model focuses on four-class classification, whereas previous studies concentrated on binary or three-class categorization. In this case, data augmentation was used to expand the dataset. In [36], end-to-end learning of a CNN-based model for three-class classification was implemented. Without specialized control, the features can be learned naturally from simple data. A convolutional autoencoder was used to transform the input data into lower-dimensional space. To identify AD [37], used a convolutional neural network that combined information from MRI and PET scans of the hippocampal area. The hippocampal area was chosen depending on the region of interest in this case (ROI). The suggested technique produces acceptable results for the categorization of AD versus CN, MCIc versus CN, and MCIc versus MCInc, because the multiple modalities are merged.

In [38], the algorithm was shown to be a powerful dual-functional 3D convolutional neural network for three-class classification and precise bilateral hippocampal segmentation. An increased classification accuracy requires accurate hippocampal segmentation. To simplify scalability while preserving segmentation accuracy, the algorithm employed V-Net convolutional blocks with a bottleneck architecture. Recent research in the field of early diagnosis of Alzheimer's disease using deep learning algorithms has been listed and analyzed in a review by [39]. This study highlights that early stage AD prediction merits far more attention than late-stage AD diagnosis. In [40], the algorithm worked with functional MRI images as well as medical information, such as age, gender, and genetic information. The deep neural network was trained using a stacked autoencoder based on functional MRI time series or correlation coefficient data. Several algorithms based on CNN and MRI in the field of early detection of Alzheimer's have been reviewed [41]. Additionally, this method presents an open framework for repeatable testing. A 3D local directional pattern was used in [42] to compute the orientation around each voxel. This algorithm was less sensitive to noise and illumination.

Hypergraph-based regularization and multi-kernel support vector machines were utilized to fuse common characteristics from diverse modalities in [43]. The results suggest that the proposed method outperforms existing multimodality strategies in terms of classification accuracy. The fundamental flaw of the algorithm is that all hyperedge weights are set to one without considering the various hyperedges. Wavelets, Gabor filters, and Gaussian local descriptors were utilized as feature extraction tools in [44] together with a support vector machine classifier. Three separate SVMs were used in the system and each was trained using different feature descriptors. Clinical and texture criteria were used in [45] to determine the mild cognitive impairment conversion stage (MCIc). The key benefit of MRI is that the entire brain texture can be used to differentiate between MCI and AD. In [46], a multivariate general linear model was used to recommend a feature-selection approach. The modest intensity fluctuations from CN to MCIc could be predicted using a general linear model. Multivariate adaptive regression splines, which are different classifiers, are also employed. Texture characteristics collected from elliptical neighborhoods provide good classification accuracy at the trade-off of a long computation time, according to [47].

MRI images were sampled with nine volumes of interest in brain regions relevant to AD [48] after preprocessing. Intensity and texture features were retrieved from the volumes of interest. An SVM classifier is used to train the features. Despite the adequate accuracy of the method, nonlinear registration schemes can be improved. Various activation functions employed in convolutional neural networks for medical purposes were compared in [49]. The efficiency of constructing pre-trained networks for medical

applications is illustrated in [50]. The approach employed in [51] is based on a deep CNN for learning both hippocampal segmentation and classification features using a 3D DenseNet. Although numerous studies have addressed the early detection of AD, it remains difficult to pinpoint the pertinent characteristics that can detect AD in its earliest stages [52]. Many of the cited studies were not concerned with the distinction between MCIc and MCInc [53]. The accuracy of studies that have accomplished the above classification is not greater than 70%.

3 Data and proposed method

This section provides an overview of the dataset employed for extracting information from MRI images, along with the proposed methods aimed at enhancing the classification accuracy for MCIc vs. MCInc. A key innovation lies in the incorporation of the well-established local binary pattern as one of the layers in the CNN architecture. The local binary pattern is renowned for its efficacy in extracting texture features. Given the subtle textural differences between stages MCIc and MCInc, capturing these gradations is crucial for achieving improved classification accuracy. The section explores into the calculation of local binary patterns, highlighting the approach of processing arrays rather than pixels individually. Furthermore, the work leverages the power of a squeeze and excitation network to further refine and enhance the classification accuracy.

3.1 Data set

In this study, MRI was used to detect Alzheimer's early. Nuclear magnetic resonance makes an MRI scan to be inherited with great clarity. MRI images were accessed from the Alzheimer's Disease Neuroimaging Initiative (ADNI) database. ADNI is the right platform for Alzheimer's disease research that makes standard MRI images available. Further research is being conducted to improve the clinical diagnosis and treatment of Alzheimer's disease. ADNI is a useful tool and an open-source dataset. This can be accessed through a link (http://adni.loni.usc.edu). It is a multi-site investigation (ADNI 1 2 3 and Go) that tracks the progression of Alzheimer's disease (AD) and its stages using clinical, imaging, and genetic biomarkers for the human brain. The dataset used in this study consists of two classes: MCIc and MCInc. The data is sourced from the ADNI dataset and consists of medical image descriptions in the DICOM format, specifically Coronal, Sagittal, and Axial views of 2D T1 weighted MRI scans. The dataset includes 150 patients classified into two categories: MCIc and MCInc, with 80 and 70 patients in each class respectively, resulting in a total of 8553 scans. The number of images for each class is as follows: MCInc (4258) and MCIc (4295). All medical data were obtained in 2D format with a size of 256×256. The images were extracted from MRI scans in MR Accelerated Sagittal MPRAGE, MR Axial Field Mapping, and MR 3 Plane Localizer views. To address the limited availability of medical datasets, traditional data augmentation techniques such as rotation and reflection (flipping) were employed to augment the original dataset. This resulted in a dataset of 17,106 images, with 8590 MCIc images and 8516 MCInc images. Data augmentation techniques were used to maximize the dataset and address the issue of overfitting. The augmented dataset of 17,106 MRI images is shuffled and split into training, and test sets using a random selection basis and a split ratio of 70:30, respectively.

3.2 Preprocessing

This study utilizes two preprocessing techniques to enhance the quality of the MRI images before feature extraction. The techniques employed are skull removal and image normalization. Skull stripping is a crucial step to remove unnecessary meningeal tissues from the MRI images. The process requires careful detection of the skull boundaries, and morphological operations such as erosion and dilation are utilized to obtain the skull-stripped image. The goal of normalization is to ensure that the pixel values have a consistent scale and distribution, which can help to improve the performance of machine learning models. This technique scales the pixel values to a specified range [0, 1]. Figure 1 displays the original MRI image alongside the normalized image and the image obtained after skull removal.

Fig. 1 From left (**a**) original image (**b**) Normalized image (**c**) image after skull removal

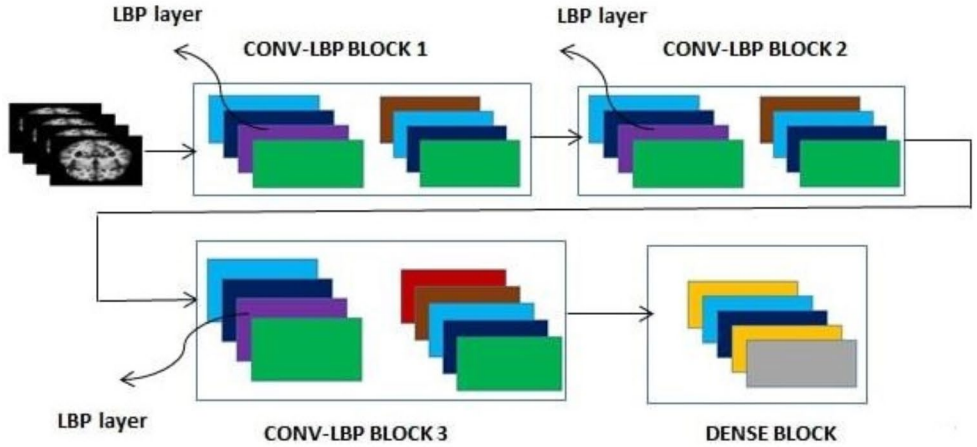

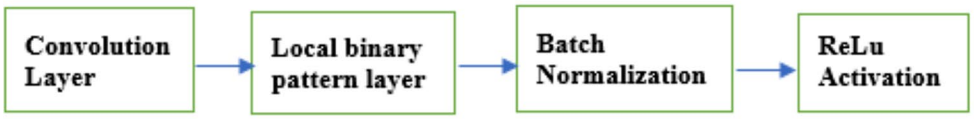

(a)

(b)

(c)

Step 1: Read MRI image

Step 2: Skull removal and Normalization

Step 3: CONV-LBP Block 1- 32 filters

Step 4: CONV-LBP Block 2 – 64 filters

Step5: CONV-LBP Block 3 – 128 filters

Step 6: Dropout Layer

Step 7: Dense Block

Step 8: MCIc vs MCInc classification

(d)

Fig. 2 Model with local binary pattern and without SENet. (**a**) CONV-LBP block – first four layers. (**b**) CONV-LBP block – second four layers. (**c**) Dense block. (**d**) Algorithm of model with LBP and without SENet

3.3 Proposed model with LBP and without SENet

A CNN is used to develop the proposed model, which includes a local binary pattern. A basic convolutional block with 32 convolutional layers, batch normalization, and an activation layer was applied to the MRI images at a size of $100 \times 100 \times 3$. Using a ReLU activation function, this stage extracts major features from the images. The feature map generated by the convolutional block was processed using a local binary pattern block, which generated a matrix-based local binary pattern. A detailed explanation of calculation of matrix-based local binary pattern is explained in the next section.

CONV-LBP BLOCK 1 is the first stage in the model shown in Fig. 2, and consists of two levels. The first level, as shows in Fig. 2a consists of a convolutional block with 32 filters, a local binary pattern, batch normalization, and the ReLu activation function (CONV + LBP + BN + ReLu). Batch normalization helps in improving the flow of gradients through the network. This is because it reduces the magnitude of the gradients and makes them more consistent, which helps in stabilizing the training process. The second level as shown in Fig. 2b consisted of a convolutional block with 32 filters, batch normalization, ReLU activation, and max pooling (CONV + BN + ReLu + Max Pooling). The CONV-LBP BLOCK 2 stage of this model is identical to the first stage except that the convolutional block uses 64 filters. The third stage, CONV-LBP BLOCK 3, consists of identical blocks as the first and second stages but with 128 filters. A dropout layer was used at the end of Stage 3 to reduce overfitting. The flattening layer, dense layer, batch normalization, activation function ReLu, and final fully connected layer for classification constitute the last stage of the DENSE BLOCK as shown in Fig. 2c. For mild cognitive impairment cognitive invertible and non-invertible classification, a dense block was designed to predict the final classification result. The feature maps are converted into a one-dimensional feature vector space using a flattened layer. These data were flattened and applied to the fully connected layers. The first and second fully connected layers had 128 and two nodes, respectively. The final output layer consisted of two output nodes for the binary categorization of the invertible and non-invertible MCI cognitive phases from the MRI images. In the final output layer, a sigmoid activation function is employed to convert the output into a probability value of 0–1. The algorithm of the model with LBP and without SENet is given in Fig. 2d.

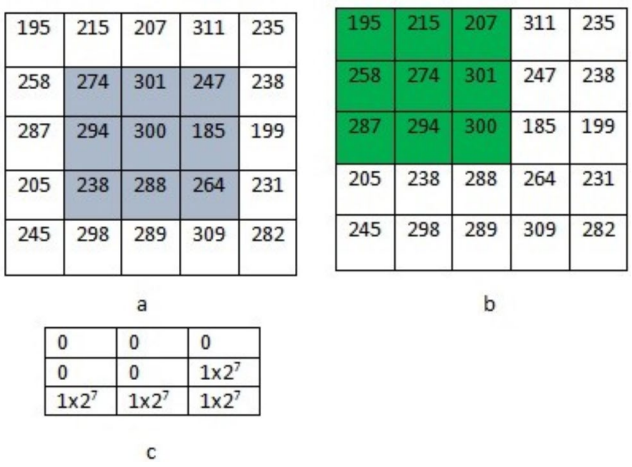

Fig. 3 Local binary pattern calculation

3.4 Local binary pattern

Local binary pattern calculations are typically performed pixel by pixel. In a 3×3 neighborhood, a central pixel is detected and compared with eight adjacent 8 pixels. A value of 1 is assigned if the neighboring pixels are greater than or equal to the central pixel; otherwise, it is 0. Following this permutation, the pixel position was multiplied by 2^0–2^7.

In this case, the local binary is calculated as an array by using an array. The center array was 3×3 array. The central array was compared with eight adjacent arrays. 2^0–2^7 are multiplied by their positions. Figure 3 shows an example of this computation. In Fig. 3, 'a' stands for a 3×3 center array. The center element of 'a' has eight adjacent pixels. Each adjacent array of 'a' consists of pixels adjacent to the center element of 'a' as the center element. Array 'b' represents an adjacent array, where 274 is the center element. Array 'c" represents the result of comparing the center array to the neighboring array, with values multiplied by 2^7. Similarly, the remaining seven adjacent arrays were used, and their values were multiplied by 2^0–2^6. The comparison strategies for the center and adjacent arrays are given by Eq. (1). Here, 'i' and j represent pixel positions. The variable 'K' stands for total number of adjacent pixels of center element in center array. Variable 'k' represents the position of the adjacent center elements in the adjacent arrays. Variable 'k' varies from 0 to 7, as eight adjacent arrays are for a 3×3 window. The sum of these eight arrays replaces the center array, as shown in Eq. (2). These operations were performed for all the elements in the convoluted image. Tex ture quality is important in the MCIc versus MCInc categorization. Consequently, using a local binary pattern in the models improved the classification accuracy.

$$\mathrm{ck(i,j)} = \begin{cases} 2\mathrm{k}, a(i,j) \geq b(i,j) \\ 0, a\,(\mathrm{i,j}) < b(i,j) \end{cases} \tag{1}$$

$$\mathrm{LBP_{array}} = \sum_{\mathrm{k}=0}^{\mathrm{K}-1} \mathrm{ck} \tag{2}$$

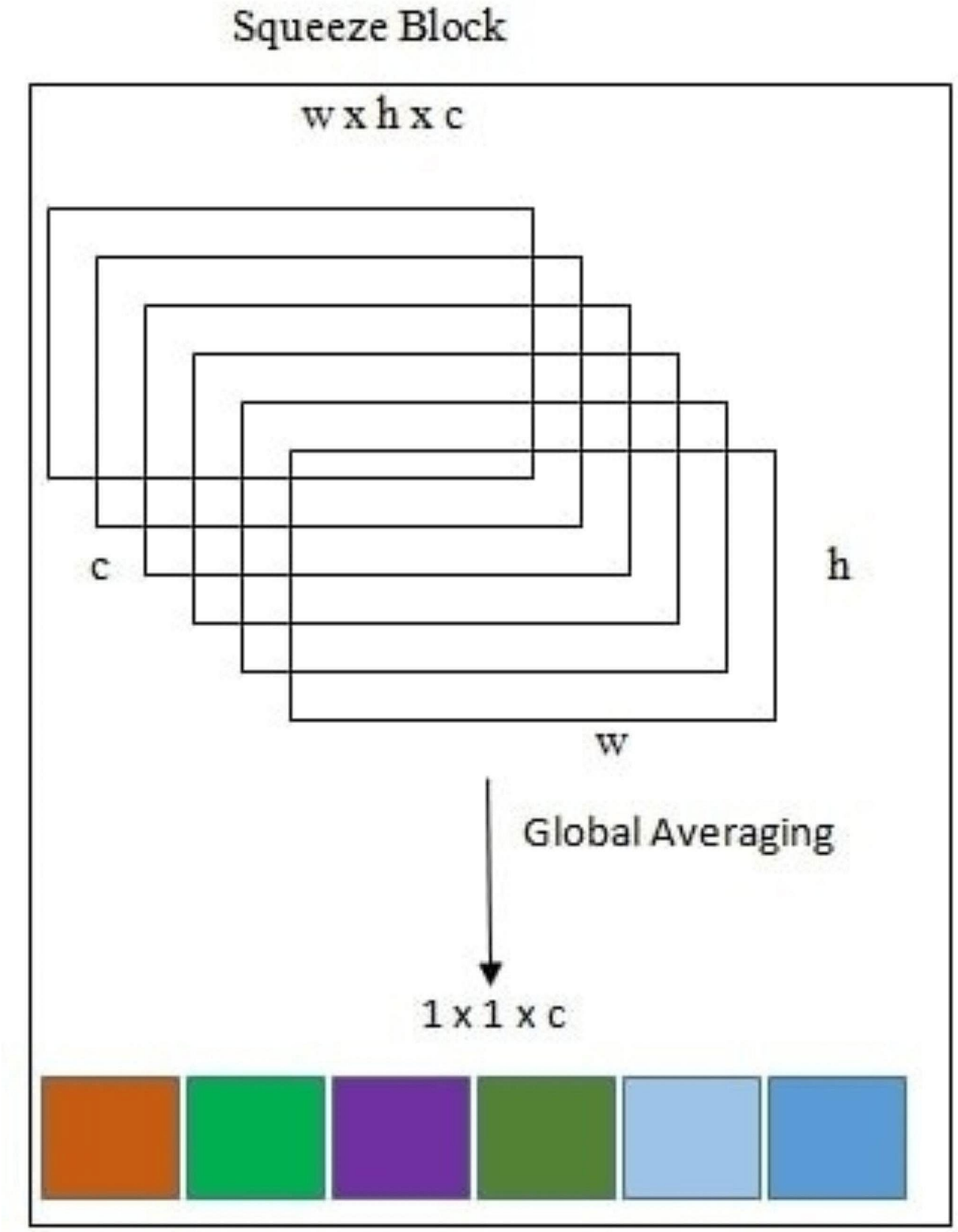

Fig. 4 Squeezing operation

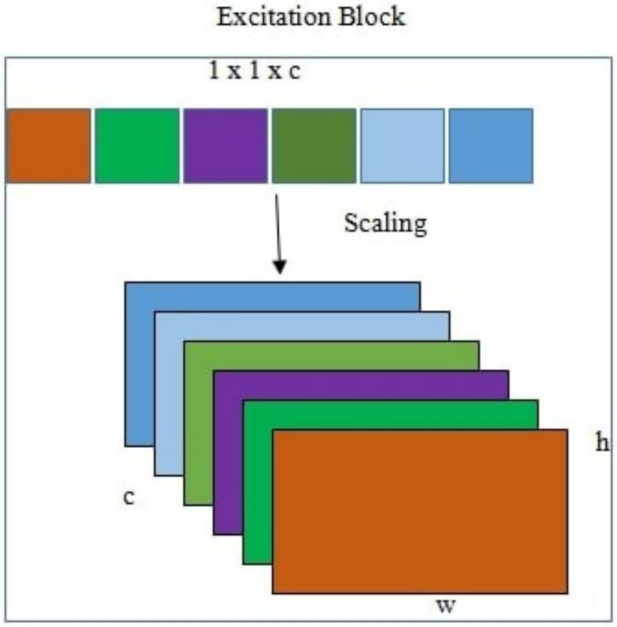

Fig. 5 Excitation operation

3.5 Proposed model with LBP and with SENet

The SENet module adaptively escalates these feature maps with a scaling factor based on their relevance after extracting first-level features. By extracting texture-based features spatially, the feature maps are squeezed into single values. These scalar values are multiplied by the input channels to scale each feature map adaptively. These feature maps were concatenated at the fusion block and excited using the rectified linear unit activation function. The squeeze and excitation network (SENet) improves channel interdependencies without significant computational effort. The weight values for each channel can be modified in this network architecture, based on the significance of the feature map. Typically, a CNN model assigns equal weight to each feature map. A linear scaling factor was applied to each channel when utilizing SENet, by squeezing the feature map values into a single numerical value. Each channel is effectively emphasized based on its relative relevance.

Consider image I of size W × H × C, where W represents the width, H represents the height, and C represents the number of channels.

$I = (i_1, i_2, i_3, \ldots\ldots\ldots, i_c)$ Each channel of image I has a size of W × H.

$I_{sq} = (isq_1, isq_2, isq_3 \ldots\ldots\ldots isq_c)$, where I_{sq} is the squeezed image representation.

$I_{ex} = (iex_1, iex_2, iex_3 \ldots\ldots iex_c)$, where Iex is the image representation after applying activation functions.

$I_{exf} = (iexf_1, iexf_2, iexf_3, \ldots. iexf_c)$ and I_{exf} is the final scaled excited image representation.

The c^{th} element of squeezed image I_{sq} can be represented as by Eq. (3)

$$isq_c = \frac{1}{W \times H} \sum_{p=1}^{W} \sum_{q=1}^{H} i_c(p, q) \tag{3}$$

Each element in the squeezed image passes through two dense layers to capture channel-wise independencies fully. isq_c is converted to iex_c as it is applied to the ReLu and sigmoid activation functions. Finally, the elements were scaled by multiplication, as shown in Eq. (4).

$$iexf_c = iex_c \times i_c \tag{4}$$

Texture properties of the brain surface are particularly important in the learning and prediction of classification results for brain MRI images. Distinct phases of mild cognitive impairment were identified using a local binary pattern that extracts texture information from MRI images. Each channel has undergone 1 × 1 parallel convolution for channel-based squeezing. Channel-by-channel pooling was performed according to the spatial pixel position, and the results were compressed into a new vector of values. Each feature map channel was spatially multiplied by this new scaling factor.

Convolutional filters were used in CNN models to extract distinct feature maps of equal relevance. However, certain feature maps provide more information than others in these feature maps. The significant feature maps are adaptively highlighted in the suggested model of a local binary pattern with SENet based on their feature-based scaling factor and the capability of the local binary pattern to retrieve texture attributes. SENet blocks separate the layers in each block, as shown in Fig. 6. The squeeze blocks process the features from level 1 of stage 1, as shown in Fig. 4. Let w, h, and c denote the image width, height, and number of channels, respectively. Using a global averaging layer, the feature maps were compressed into single values. The feature map is 1 × 1 × c after squeezing. The resultant scalar values, 1 × 1 × c, were multiplied by the input channels in the excitation block, as illustrated in Fig. 5, to adaptively scale each feature map. Level 2 of Stage 1 receives the features collected from the SENet block. These steps were repeated for the remaining two stages. The algorithm of model with LBP and SENet is given in Fig. 6a.

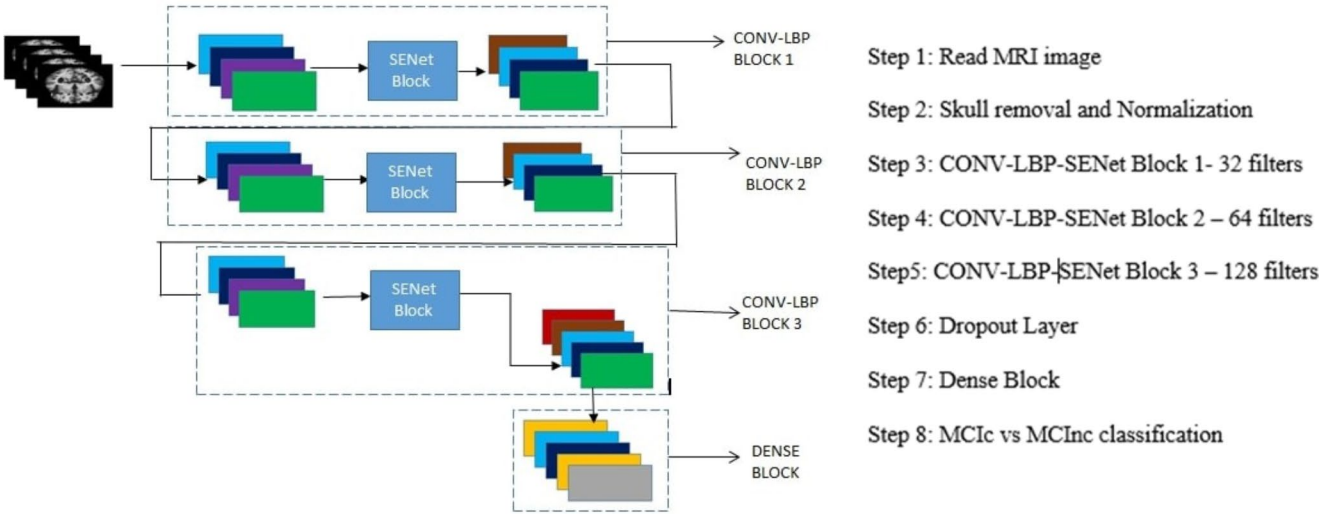

Fig. 6 Model with local binary pattern and SENet. (**a**) Algorithm of model with LBP and SENet

4 Results

The suggested model was examined individually with and without the SENet block, and the results were obtained. Only the mild cognitive impairment convertible and non-convertible phases were used to train and evaluate the model. According to the literature, the categorization accuracy of Alzheimer's disease and cognitively normal images is approximately 100%. Other classifications, such as MCIc vs. CN and the four phases of categorization, had little effect on early Alzheimer's disease identification. Alzheimer's disease can be diagnosed early if and only if the illness is detected at the MCIc level. A person's path to AD looks as follows: CN, MCInc., MCIc, and AD. Therefore, the accuracy of MCIc vs. MCInc classification is crucial. Therefore, this study focused more on the MCIc versus MCInc classification.

This research was programmed using Python language version 3.6 and the Keras library [54, 55]. Keras is a high-level open-source machine learning library that is written in Python and is specifically designed for easy and efficient implementation of deep learning models. It is commonly used for numerical computation tasks and enables users to perform computations with ease and efficiency. The MRI images were obtained from the ADNI dataset. Subsequently, the images were subjected to data augmentation to avoid overfitting. 70% of the images were used to train the model. The remaining 30% of the images were used for testing. For the validation, 10% of the training images were used. For testing, 2577 MCIc MRI images and 2555 MCInc images were used. The size of the input MRI images, 256×256, was limited to 100×100. The proposed model was applied to the preprocessed images. The model was optimized using the stochastic gradient descent method. The implementation uses a learning rate of 0.01. The model takes advantage of SENet and a local binary pattern. The computational complexity was reduced using a tensor-based local binary pattern, as shown in Fig. 3. SENet extracts features with a minimal computational effort. This helps fuse the spatial and channel information of the images. The first model (Fig. 2) had a total of 1,673,249 parameters, with 1,672,097 being trainable and 1,152 being non-trainable. The second model (Fig. 6) had a total of 1,673,991 parameters, with 1,672,839 being trainable and 1,152 being non-trainable. When trained with 1,673,249 total parameters, the first model achieved a classification accuracy of 82%. In contrast, the second model, which incorporated SENet and had 1,673,991 total parameters, achieved a higher accuracy of 86%. If regular CNN elements were used instead of SENet to improve the first model's accuracy beyond 82%, the number of trainable parameters would exceed 1,673,991, highlighting the advantage of using SENet in this context. Many studies in this field have not focused on the MCIc vs. MCInc classification accuracy. The studies being discussed have a low accuracy rate of approximately 70%. The proposed model outperformed existing techniques for the classification of MCIc vs. MCInc. The model shown in Fig. 2 had a classification accuracy of 82%. According to the model shown in Fig. 5, the use of SENet improved the classification accuracy to 86%.

The classification performance was assessed using measures such as recall, precision, and f1-score, in addition to accuracy, as given in Eqs. (5), (6), (7), and (8). True-positive, false-positive, true-negative, and false-negative classifications are represented by TP, FP, TN, and FN, respectively.

$$\text{Precision} = \frac{\text{TP}}{\text{TP} + \text{FP}} \tag{5}$$

Table 1 Classification report for MCIc vs. MCInc without SENet

	Precision	Recall	f1-score	Support
MCIc	0.80	0.84	0.82	2577
MCInc	0.83	0.79	0.81	2555

Table 2 Classification report for MCIc vs. MCInc with SENet

	Precision	Recall	f1-score	Support
MCIc	0.84	0.90	0.87	2577
MCInc	0.89	0.83	0.85	2555

Table 3 Performance analysis of proposed models

	Precision	Recall	f1-score	Accuracy (%)
LBP without SENet	0.82	0.82	0.82	82
LBP with SENet	0.86	0.86	0.86	86

Table 4 Comparison of classification accuracy (%)

Method	MCIc vs. MCInc
Proposed method	**86**
Local Binary Pattern + CNN [57]	68.70
VoxlMG + SVM [44]	67.10
Hypergraph + SVM [43]	68.52
Ensemble learning + convolutional neural network [34]	62.06
Multimodality + CNN [56]	76.90

$$\text{Recall} = \frac{\text{TP}}{\text{TP} + \text{FN}} \tag{6}$$

$$\text{Accuracy} = \frac{\text{TP} + \text{TN}}{\text{TP} + \text{TN} + \text{FP} + \text{FN}} \tag{7}$$

$$\text{f1} - \text{score} = 2 * \frac{(\text{Precision}*\text{Recall})}{\text{Precision} + \text{Recall}} \tag{8}$$

The classification report consisted of the recall, precision, f1-score, and accuracy of both models, as shown in Tables 1 and 2, and 3.

The results were compared with the classification accuracy of MCIc vs. MCInc in the literature, as shown in Table 4. As stated previously, only the classification accuracy of MCIc vs. MCInc was considered for comparison. The classification accuracy of MCIc versus MCInc was 67.1% [54] using voxels, feature selection, and a support vector machine. Hypergraph-based multimodal classification [43] provided a classification accuracy of 75.48%. However, both magnetic resonance imaging (MRI) and positron emission tomography (PET) modalities been used. The same algorithm works on single-modality MRI and provides a classification accuracy of 68.52%. The two-stage ensemble learning method proposed in [34] provided a classification accuracy of 62.06%. In [56], 3D CNN-based multimodal classification was performed, and the classification accuracy of MCIc vs. MCInc. was 76.90%. The proposed model with and without SENet yielded an accuracy of 82%, whereas that with LBP and SENet yielded an accuracy of 86%. In [57], the fast Hessian matrix was used to identify significant points in MRI images, and the local binary pattern was then used to describe the key points of the fast Hessian detector. Because the dimensionality is very high, principal component analysis is utilized to reduce the feature length for computational efficiency. CNNs have been used to anticipate various stages of AD. For both MCIc vs. CN and AD vs. CN, the classification accuracy of the algorithm was good. However, the classification accuracy of MCIc versus MCInc could still be improved. The combined use of LBP features and CNN improved the classification accuracy of MCIc versus CN, and AD versus CN. However, when LBP is incorporated as a CNN layer, deep learning that corrects the error enables the proposed system to provide improved classification accuracy for MCIc vs. MCInc. The performance of the proposed model was compared with that of other prominent algorithms in the literature.

The confusion matrices show the difference between the expected and observed values. In the confusion matrix of model MCIc vs. MCInc without SENet shown in Figs. 7 and 2175 stands for correctly identified MCIc images out of the 2577 samples. Similarly, 2026 represents correctly identified MCInc images out of 2555 images. Results 402 and 529 represent falsely identified MCIc and MCInc images, respectively, and denote the number of real negative cases categorized as positive and real positive examples classified as negative, respectively. Similarly, in the confusion matrix with SENet shown in Figs. 7 and 2307 stands for correctly identified MCIc images out of the 2577 samples. Similarly, 2108 stands for correctly identified MCInc images out of 2555 images. The 270 and 447 results represent falsely identified MCIc and MCInc images, respectively, and denote the number of real negative cases categorized as positive and real positive examples classified as negative, respectively.

The ROC curve area denotes the two-dimensional area beneath the complete ROC curve from (0,0) to (1,1). The area has a value of 0–1. The values of 0 and 1 indicate whether the model's predictions are correct or incorrect, respectively. The area under the ROC curve was 0.92 for the model without SENet and 0.95 for the model with local binary pattern and SENet in this study. The ROC curves for the models with and without the SENet are shown in Fig. 8.

5 Discussions

The model, incorporating both the local binary pattern and squeeze-and-excitation network, demonstrates superior classification accuracy when compared to existing methods.

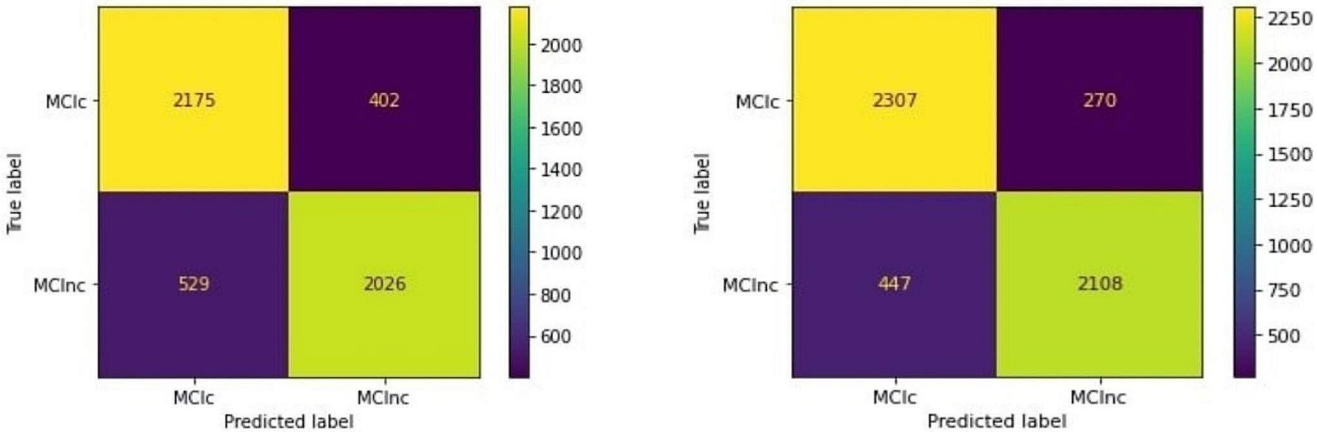

Fig. 7 Confusion matrix: MCIc vs. MCInc without SENet (left) and MCIc vs. MCInc with SENet (right)

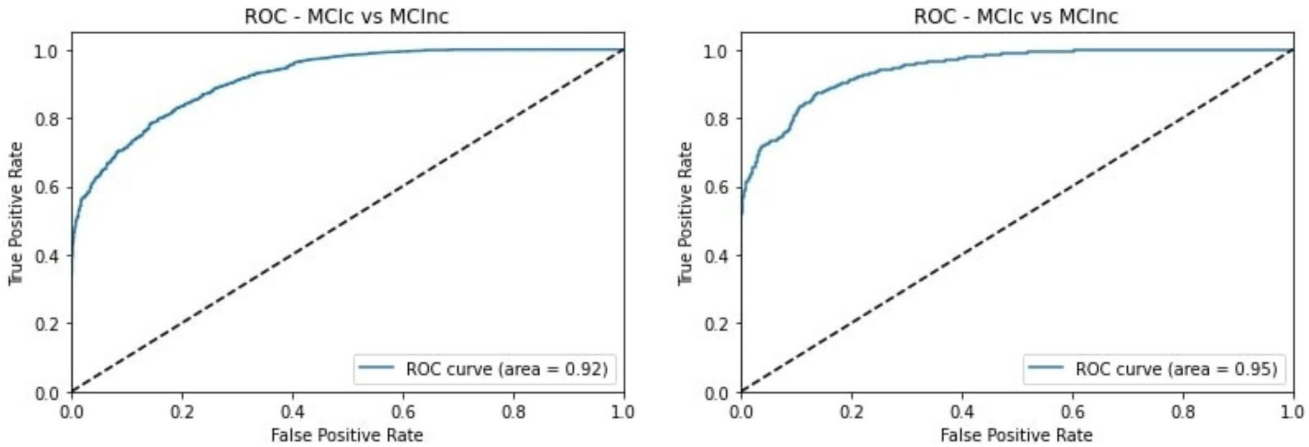

Fig. 8 Receiver Operating Characteristics: MCIc vs. MCInc without SENet (left) and MCIc vs. MCInc with SENet (right)

Notably, the computational cost of local binary pattern calculation is addressed in this work. In contrast to the pixel-by-pixel approach outlined in [57], which is difficult, the local binary pattern calculations are executed array by array, resulting in a more computationally efficient process.

The inclusion of the squeeze-and-excitation network contributes to the overall computational efficiency of the model. This network effectively compresses important features and enhances each pixel with the condensed value. Achieving equivalent classification accuracy with other models [34, 56] necessitates the use of additional layers in the absence of the SENet. In contrast, our model, leveraging SENet with fewer layers, emphasizes crucial features, a factor advantageous for classification purposes. Furthermore, potential complexity reduction is achievable by minimizing the number of local binary pattern layers.

The study also includes a comparative analysis of the classification accuracy between the base model without local binary pattern and squeeze-and-excitation network (SENet) and the models incorporating local binary pattern and SENet. The classification accuracy of the base model, lacking both LBP and SENet, is observed to be less noteworthy.

6 Conclusion

Early AD detection gives patients and their relatives the opportunity to take all the necessary precautions before the situation becomes serious. Medical professionals can prescribe drugs to reduce brain atrophy. A deep learning model that combines the strengths of the well-known LBP texture operator and SENet is proposed in this study for the early detection of AD. The characteristics of the LBP descriptor were incorporated as a convolutional neural network layer to improve classification accuracy. SENet can extract global features with minimal computational effort. The textural properties of the local binary patterns and computational efficiency of SENet enabled the proposed system to achieve a classification accuracy of 86% between MCIc and MCInc. As given in the literature, more emphasis should be placed on the classification of MCIc and MCInc. The suggested

approach is both efficient and appropriate in terms of MCIc vs. MCInc classification. A unique strategy for classifying mild cognitive impairment into convertible and non-convertible stages is proposed in this study.

7 Future work

The suggested model has the potential for future extensions to incorporate various local binary patterns, with a focus on evaluating its classification performance. Additionally, there is scope for further reduction in computational complexity by integrating a single local binary pattern layer and a squeeze-and-excitation network layer alongside CNN. Furthermore, it is essential for the model to be encapsulated within a callable function, enabling the simultaneous execution of convolution and local binary pattern extraction to extract the predominant features from input images.

Acknowledgements We would like to thank all of our universities, institutes, and organizations for facilitating our time support in this study.

Authors contribution Contributors A.F., I.A.P and H.D. conceived and designed the research, and A.F., I.A.P, A.J, K.M.S and H.D. wrote the first draft of the manuscript. L.D., M.P and Li.D. all contributed in a substantial way to the writing process. All the authors revised the manuscript. All authors read and approved the final version of the manuscript.

Data availability The datasets used in this study were obtained from the Alzheimer's Disease Neuroimaging Initiative (ADNI) database. This was an open-access dataset available from the link (http://adni.loni.usc.edu).

Declarations

Ethical and informed consent Not applicable.

Competing interests The authors declare that they have no competing.

References

1. Breijyeh Z, Karaman R (2020) Comprehensive review on Alzheimer's disease: causes and treatment. Molecules 25(24):5789. https://doi.org/10.3390/molecules25245789
2. Mendez MF (2012) Early-onset Alzheimer's disease: nonamnestic subtypes and type 2 AD. Arch Med Res 43(8):677–685. https://doi.org/10.1016/j.arcmed.2012.11.009
3. Zhu D, Montagne A, Zhao Z (2021) Alzheimer's pathogenic mechanisms and underlying sex difference. Cell Mol Life Sci 78(11):4907–4920
4. Hien DTT, Huan HX, Huynh HT (2009) Multivariate interpolation using radial basis function networks. Int J Data Min Modelling Manage 1(3):291–309
5. Thusnavis Bella Mary I, Bruntha PM, Manimekalai MAP, Sagayam KM, Dang H (2021) Investigation of an efficient Integrated Semantic interactive algorithm for image Retrieval. Pattern Recognit Image Anal 31(4):709–721
6. Hien DTT, Huan HX, Hoang LXM (2015) An effective solution to regression problem by RBF neuron network. Int J Oper Res Inform Syst (IJORIS) 6(4):57–74
7. Rajesh G, Raajini XM et al (2020) A statistical approach for high order epistasis interaction detection for prediction of diabetic macular edema. Inf Med Unlocked 20:100362. https://doi.org/10.1016/j.imu.2020.100362
8. Elayaraja P, Kumarganesh et al (2022) An efficient approach for detection and classification of cancer regions in cervical images using optimization based CNN classification approach. J Intell Fuzzy Syst 43(1):1023–1033
9. Jebarani PE, Umadevi N et al (2021) A Novel Hybrid K-Means and GMM Machine learning model for breast Cancer detection. IEEE Access 9:146153–146162. https://doi.org/10.1109/ACCESS.2021.3123425
10. Sundar GN, Narmadha D et al (2021) Automated sleep stage classification in sleep apnoea using convolutional neural networks, Informatics in Medicine Unlocked. Volume 26, 100724 (2021). https://doi.org/10.1016/j.imu.2021.100724
11. Rajesh G, Raajini XM et al (2020) A statistical approach for high order epistasis interaction detection for prediction of diabetic macular edema. Inf Med Unlocked 20:100362
12. Balwant MK (2022) A review on convolutional neural networks for Brain Tumor Segmentation: methods, datasets, libraries, and future directions. IRBM 43(6):521–537 -CNN
13. Dequidt P, Bourdon P, Tremblais B, Guillevin C, Gianelli B, Boutet C, Cottier JP, Vallée JN, Fernandez-Maloigne C, Guillevin R (2021) Exploring radiologic criteria for glioma grade classification on the BraTS dataset. IRBM 42(6):407–414 – SVM, BRAIN TUMOR CLASIFICATION
14. Khairandish MO, Sharma M, Jain V, Chatterjee JM, Jhanjhi NZ (2022) A hybrid CNN-SVM threshold segmentation approach for tumor detection and classification of MRI brain images. IRBM 43(4):290–299 – CNN AND SVM
15. Angulakshmi M, Priya GL (2019) Walsh Hadamard transform for simple linear iterative clustering (SLIC) superpixel based spectral clustering of multimodal MRI brain tumor segmentation. IRBM 40(5):253–262 – MRI images, texture based super pixels
16. Zhang Y, Duan J, Sa Y, Guo Y (2022) Multi-atlas based adaptive active contour model with application to organs at risk segmentation in brain mr images. IRBM 43(3):161–168 MRI images
17. Singh VR (2008) Ultrasound hyperthermia control system for deep-seated tumours: ex vivo study of excised tumours, modeling of thermal profile and future nanoengineering aspects. IRBM 29(5):326–336 Medical application
18. Wischhusen J, Padilla F (2019) Ultrasound-targeted microbubble destruction (UTMD) for localized drug delivery into tumor tissue. IRBM 40(1):10–15 MEDICAL APPICATION
19. Caredda C, Mahieu-Williame L, Sablong R, Sdika M, Guyotat J, Montcel B (2021) Real time intraoperative functional brain mapping based on RGB Imaging. IRBM 42(3):189–197
20. Dolz J, Massoptier L, Vermandel M (2015) Segmentation algorithms of subcortical brain structures on MRI for radiotherapy and radiosurgery: a survey. Irbm 36(4):200–212
21. Gupta V, Mittal M, Mittal V, Sharma AK, Saxena NK (2021) A novel feature extraction-based ECG signal analysis. J Institution Eng (India): Ser B 102(5):903–913
22. Gupta V, Mittal M, Mittal V (2022 May) A novel FrWT based arrhythmia detection in ECG signal using YWARA and PCA. Wireless Pers Commun 1:1–8
23. Andrew J, Mhatesh et al (2021) Super-resolution reconstruction of brain magnetic resonance images via lightweight autoencoder. Inf Med Unlocked 26:100713

24. Andrushia AD, Sagayam KM et al (2021) Visual-saliency-based abnormality detection for MRI brain images-Alzheimer's Disease Analysis. Appl Sci 11(19). https://doi.org/10.3390/app11199199
25. Fathi S, Ahmadi M, Dehnad A (2022) Early diagnosis of Alzheimer's disease based on deep learning: a systematic review. Comput Biol Med 105634. https://doi.org/10.1016/j.compbiomed.2022.105634
26. Francis A, Pandian IA (2021) Early detection of Alzheimer's disease using ensemble of pre- trained models. In2021 International Conference on Artificial Intelligence and Smart Systems (ICAIS) 2021 Mar 25, pp. 692–696. IEEE
27. Suk HI, Shen D (2013) Deep learning-based feature representation for AD/MCI classification. In- International Conference on Medical Image Computing and Computer-Assisted Intervention 2013 Sep 22, pp. 583–590. Springer, Berlin, Heidelberg
28. Payan A, Montana G (2013) Predicting Alzheimer's disease: a neuroimaging study with 3D convolutional neural networks. arXiv Preprint arXiv :150202506
29. Gupta A, Ayhan M, Maida A (2013) Natural image bases to represent neuroimaging data. In International conference on machine learning 2013 Feb 13, pp. 987–994
30. Valliani A, Soni A (2017) Deep residual nets for improved Alzheimer's diagnosis. In Proceedings of the 8th ACM International Conference on Bioinformatics, Computational Biology, and Health Informatics 2017 Aug 20, pp. 615–615
31. He K, Zhang X, Ren S, Sun J (2016) Deep residual learning for image recognition. In Proceedings of the IEEE conference on computer vision and pattern recognition. pp. 770–778 (2016)
32. McCrackin L (2018) Early detection of Alzheimer's Disease using deep learning. In: Bagheri E, Cheung J (eds) Advances in Artificial Intelligence. Canadian AI 2018. Lecture notes in Computer Science(), vol 10832. Springer, Cham, pp 355–359. https://doi.org/10.1007/978-3-319-89656-4_40.
33. Jain R, Jain N, Aggarwal A, Hemanth DJ (2019) Convolutional neural network based Alzheimer's disease classification from magnetic resonance brain images. Cogn Syst Res 57:147–159
34. Pan D, Zeng A, Jia L, Huang Y, Frizzell T, Song X (2020) Early detection of Alzheimer's Disease using magnetic resonance imaging: a Novel Approach combining Convolutional neural networks and ensemble learning. Front NeuroSci, 14
35. Islam J, Zhang Y (2018) Brain MRI analysis for Alzheimer's disease diagnosis using an ensemble system of deep convolutional neural networks. Brain Inf 5(2):2
36. Oh K, Chung YC, Kim KW et al (2019) Classification and visualization of Alzheimer's Disease using volumetric convolutional neural network and transfer learning. Sci Rep 9:18150. https://doi.org/10.1038/s41598-019-54548-6
37. Huang Y, Xu J, Zhou Y, Tong T, Zhuang X, Alzheimer's Disease Neuroimaging Initiative (ADNI) (2019) Diagnosis of Alzheimer's disease via multi-modality 3D convolutional neural network. Front NeuroSci 13:509
38. Sun J, Yan S, Song C, Han B (2020) Dual-functional neural network for bilateral hippocampi segmentation and diagnosis of Alzheimer's disease. Int J Comput Assist Radiol Surg 15(3):445–455
39. Al-Shoukry S, Rassem TH, Makbol NM (2020) Alzheimer's diseases detection by using Deep Learning algorithms: a Mini-review. IEEE Access 8:77131–77141
40. Ju R, Hu C, Li Q (2017) Early diagnosis of Alzheimer's disease based on resting-state brain networks and deep learning. IEEE/ACM Trans Comput Biol Bioinf 16(1):244–257
41. Wen J, Thibeau-Sutre E, Diaz-Melo M et al (2020) Alzheimer's Disease Neuroimaging Initiative. Convolutional neural networks for classification of Alzheimer's disease: overview and reproducible evaluation. Med Image Anal 63:101694. https://doi.org/10.1016/j.media.2020.101694
42. Yan S, Song C, Zheng B (2019) 3D local directional patterns for early diagnosis of Alzheimer's disease. J Eng 2019(14):530–535
43. Shao W, Peng Y, Zu C, Wang M, Zhang D (2020) Alzheimer's Disease Neuroimaging Initiative. Hypergraph based multi-task feature selection for multimodal classification of Alzheimer's disease. Comput Med Imaging Graph 80:101663
44. Nanni L et al (2019) Texture descriptors and voxels for the early diagnosis of Alzheimer's disease. Artif Intell Med 97:19–26
45. Luk CC et al (2018) Alzheimer's disease: 3-Dimensional MRI texture for prediction of conversion from mild cognitive impairment. Alzheimer's Dementia: Diagnosis Assess Disease Monit 10:755–763. https://doi.org/10.1016/j.dadm.2018.09.002
46. C¸ evik A et al (2017) Voxel-MARS: a method for early detection of Alzheimer's disease by classification of structural brain MRI. Annals of Operations Research 258.1 : 31–57 (2017)
47. Nanni L, Brahnam S, Maguolo G (2019) Data augmentation for building an ensemble of convolutional neural networks. Innovation in Medicine and Healthcare Systems, and Multimedia. Springer, Singapore, pp 61–69
48. Chincarini A, Bosco P, Gemme G et al (2014) Automatic temporal lobe atrophy assessment in prodromal AD: data from the DESCRIPA study. Alzheimer's Dement 10(4):456–467
49. Maguolo G, Nanni L, Ghidoni S (2019) Ensemble of Convolutional Neural Networks Trained with different activation functions. arXiv preprint arXiv:1905.02473
50. Nanni L, Ghidoni S, Brahnam S (2021) Ensemble of convolutional neural networks for bioimage classification. Appl Comput Inf 17(1):19–35. https://doi.org/10.1016/j.aci.2018.06.002
51. Liu M et al (2020) A multi-model deep convolutional neural network for automatic hippocampus segmentation and classification in Alzheimer's disease. Neuro Image 208 : 116459 (2020). https://doi.org/10.1016/j.neuroimage.2019.116459
52. Kavitha C, Mani V, Srividhya SR et al (2022) Early-stage Alzheimer's Disease Prediction using machine learning models. Front Public Health 10. https://doi.org/10.3389/fpubh.2022.853294
53. Francis A, and Immanuel Alex Pandian (2018). Review on Local Feature Descriptors for Early Detection of Alzheimer's Disease. 2018 International Conference on CircuitsSystems in Digital Enterprise Technology (ICCSDET). IEEE
54. François C (2015) Keras: The Python deep learning library. keras. io : 86
55. Chollet F et al (2021) Keras (Version 2.6) [Computer software]. GitHub
56. Huang Y, Xu J, Zhou Y, Tong T, Zhuang X, Alzheimer's Disease Neuroimaging Initiative (ADNI) (2019). Diagnosis of Alzheimer's disease via multi-modality 3D convolutional neural network. Front NeuroSci, 509
57. Francis A, Pandian IA (2021) Early detection of Alzheimer's disease using local binary pattern and convolutional neural network. Multimedia Tools Appl 80(19):29585–29600